HYDROLOGICAL PROCESSES
Hydrol. Process. **28**, 1507–1524 (2014)
Published online 29 January 2013 in Wiley Online Library
(wileyonlinelibrary.com) DOI: 10.1002/hyp.9683

A multimodel comparison for assessing water temperatures under changing climate conditions via the equilibrium temperature concept: case study of the Middle Loire River, France

Vincent Bustillo,[1,2]* Florentina Moatar,[2] Agnès Ducharne,[3] Dominique Thiéry[4] and Alain Poirel[5]

[1] *Université François-Rabelais de Tours, EA 6293 GéHCO Géo-Hydrosystèmes Continentaux, Parc de Grandmont 37200 Tours, France*
[2] *CESBIO UMR 5126 (CNES-CNRS-IRD-UPS), IUT Paul Sabatier, Antenne d'Auch-24, rue d'Embaquès 32000 Auch, France*
[3] *UMR 7619 Sisyphe, Université Pierre et Marie Curie/CNRS, Boite 105-4 Place Jussieu-75252 , Paris Cedex 05, France*
[4] *Bureau de Recherches Géologiques et Minières (BRGM), 3 avenue Claude-Guillemin-BP 36009 45060 Orléans Cedex 2, France*
[5] *EDF/DTG, 21, av. de l'Europe-BP 41-38040 Grenoble Cedex, France*

Abstract:

This paper investigates three categories of models that are derived from the equilibrium temperature concept to estimate water temperatures in the Loire River in France and the sensitivity to changes in hydrology and climate. We test the models' individual performances for simulating water temperatures and assess the variability of the thermal responses under the extreme changing climate scenarios that are projected for 2081–2100. We attempt to identify the most reliable models for studying the impact of climate change on river temperature (T_w). Six models are based on a linear relationship between air temperatures (T_a) and equilibrium temperatures (T_e), six depend on a logistic relationship, and six rely on the closure of heat budgets. For each category, three approaches that account for the river's thermal exchange coefficient are tested. In addition to air temperatures, an index of day length is incorporated to compute equilibrium temperatures. Each model is analysed in terms of its ability to simulate the seasonal patterns of river temperatures and heat peaks. We found that including the day length as a covariate in regression-based approaches improves the performance in comparison with classical approaches that use only T_a. Moreover, the regression-based models that rely on the logistic relationship between T_e and T_a exhibit root mean square errors comparable (0.90 °C) with those obtained with a classical five-term heat budget model (0.82 °C), despite a small number of required forcing variables. In contrast, the regressive models that are based on a linear relationship $T_e = f(T_a)$ fail to simulate the heat peaks and are not advisable for climate change studies. The regression-based approaches that are based on a logistic relationship and the heat balance approaches generate notably similar responses to the projected climate changes scenarios. This similarity suggests that sophisticated thermal models are not preferable to cruder ones, which are less time-consuming and require fewer input data.

KEY WORDS thermal models; climate changes; equilibrium temperature; Loire River

Received 4 May 2012; Accepted 11 December 2012

INTRODUCTION

River temperature is a key parameter for the ecological responses of aquatic organisms. Not only does this parameter influence the O_2 content of water (Sand-Jensen and Pedersen, 2005), but it also affects the consumption rates of nutrients by organisms, potentially leading to alterations in water quality during instances of increasing temperatures. Warming also modifies the distributions and dynamics of aquatic species across hydrographic networks (Eaton and Scheller, 1996; Boisneau *et al.*, 2008). For example, recent climate warming enhances thermal stress for fish populations and tends to restrict their summer habitats drastically (Headrick and Carline, 1993).

River temperatures are driven by both natural and anthropogenic factors. The main natural factors have been thoroughly identified. These factors include incoming radiation; microclimatic features (Johnson, 2003), such as wind sheltering, shadowiness (e.g. St-Hilaire *et al.*, 2000) and local humidity deficits that are related to surrounding reliefs, the shapes of valleys, and river widths; and catchment topography and stream orientations (Sridhar *et al.*, 2004) that determine spatial patterns in river temperature changes, which may differ significantly from those of driving meteorological variables (Webb *et al.*, 2008). Other factors are groundwater inputs (e.g. chalk streams; Mackey and Berry, 1991); cold-water sources from melting snow; hydrological features, such as the mean river depths associated with river flows (e.g. the Loire River; Moatar and Webb *et al.*, 2003; Gailhard, 2006; Webb and Nobilis, 2007) and their regulation (Webb and Walling, 1997); the residence times within a hydrographic network (e.g. Gu and Li, 2002); and river's connectivity with a hyporheic zone (Evans and Petts, 1997; Hannah *et al.*, 2009). Anthropogenic influences are associated with disturbances in rivers' hydraulics (e.g. manmade levees: Bartholow *et al.*, 2004; regulating reservoirs: Webb and Walling, 1997; Poirel *et al.*, 2009), warm-water input from wastewater (Kinouchi *et al.*, 2007) and/or power plants (Poulin, 1980), forest clearing

*Correspondence to: Vincent Bustillo, Université Paul Sabatier, IUT Paul Sabatier, CESBIO UMR 5126 (CNES-CNRS-IRD-UPS), 24 rue d'Embaquès, 32000 Auch, France.
E-mail: vincent.bustillo@iut-tlse3.fr

(Sridhar *et al.*, 2004; Moore *et al.*, 2005), and anthropogenic global warming that affects hydrological regimes and near-surface meteorological variables (Mohseni *et al.*, 1999).

A broad range of thermal models for rivers

Several modelling approaches are commonly employed to simulate river temperatures. Statistical models (e.g. Mohseni *et al.*, 1998; Webb *et al.*, 2003; Caissie *et al.*, 2005; Ducharne, 2008) are based on variables that are correlated with water temperatures. Air-to-water relationships are commonly used, but many other variables may be included, such as geomorphic, riparian, and catchment characteristics (Wehrly *et al.*, 2009). New statistical approaches have been tested recently, including spectral analysis (Steel and Lange, 2007), geostatistical methods that are based on the analysis of temporal covariance structures (e.g. Gardner and Sullivan, 2004), evolutionary polynomial regressions (Giustolisi *et al.*, 2007), and artificial neural networks (Sivri *et al.*, 2007; Chenard and Caissie, 2008; Bélanger *et al.*, 2005). Stochastic approaches use autoregressive techniques that account for the departure of river temperatures from seasonal standards and have also been widely applied (e.g. Caissie *et al.*, 1998) since the pioneering work of Cluis (1972). Deterministic models consist of attempts to solve the heat budget equation (e.g. St-Hilaire *et al.*, 2003; Caissie *et al.*, 2007). These methods are intensively applied to studying the thermal regimes of individual stream reaches, but their implementation requires reach-specific input data, such as the stream geometries of hydrological features, which are rarely available. However, these methods are widely used to investigate the impacts of climate change and other anthropogenic pressures (e.g. forest harvesting, river restoration, and dam building) on the thermal regimes of river reaches with a particular attention to thermal refugia (Sinokrot *et al.*, 1995; Burkholder *et al.*, 2008). These models typically account for five heat terms that are linked directly to climate: net solar radiation, atmospheric radiation, long-wave radiation emitted by water, air–water convection (or sensible heat flux), and evaporation/condensation (or latent heat flux). The calculation of these terms depends on several near-surface meteorological variables: air temperature, air humidity, wind speed, and global and atmospheric radiation. This suite of intensive input data is frequently not available and led to the development of simplified models.

The equilibrium temperature concept

Thermal modelling may be achieved via the equilibrium temperature concept (Edinger, 1968), which is recognized as an appealing way to simulate river temperatures (Caissie *et al.*, 2005). The two central variables are the equilibrium temperature (T_e) and the heat exchange coefficient (K_e). The equilibrium temperature (T_e) is defined as the water temperature (T_w) at which the net rate of heat exchange at the interface of the water body is 0. The thermal exchange coefficient (K_e) is the rate at which the water temperature responds to heat exchange processes. T_e can be deduced from the aforementioned meteorological variables, but it also can be approximated as a function of air temperature (Mohseni *et al.*, 1998; Caissie *et al.*, 2005). T_e may be defined empirically with a small number of forcing variables (e.g. air temperature only), which allows one to overcome the frequent issue of near-surface meteorological variables being not entirely available or poorly estimated. The latter case may apply not only to long-term historical time series but also to climatic projections. For example, Räisänen (2007) argued that the agreement on recent changes in air temperature, which is simulated by 21 general circulation models (GCMs), is much stronger than the consensus for any other meteorological variable.

Under the simplifying hypothesis that K_e is constant over the course of a day, the equilibrium temperature concept enables the assessment of the short-term variability of each temperature (subdaily) with reasonable calculation requirements (Edinger *et al.*, 1968) that are less numerous than those of the classical 0D physically based model. Moreover, these concepts provide an efficient tool for achieving thermal modelling with low-frequency forcing data because the data can be rearranged into an explicit equation that is straightforward to solve and is unconditionally stable. Because air temperature (T_a) is a good predictor of water temperature (e.g. Stefan and Preud'homme, 1993; Webb and Nobilis, 1997; Caissie *et al.*, 1998; Ducharne, 2008) and thus of equilibrium temperature, several regression-based approaches are employed to account for the $T_e = f(T_a)$ relationships. The investigations from Caissie *et al.* (2005) on the Catamaran Brook in Canada suggest that in this specific case, the equilibrium temperature T_e might reasonably be assessed by means of a linear relation with air temperature and that the thermal exchange coefficient might be considered constant. However, when these simplified methods are applied to input data very distinct from those involved in the calibration of the model, it is questionable whether they indeed remain valid. Mohseni *et al.* (1998) showed that the air-to-water temperature relationship calculated with weekly datasets departs from linearity above 25 °C, and therefore, the method proposed by Caissie *et al.* (2005) is not applicable for this range of temperature. This feature is a critical issue for the accurate prediction of thermal impacts, whether from climate change, from microclimatic changes associated with the clear-cutting of riparian forests, or from the drastic modifications of hydrological regimes that are related to climate change, for example, agricultural pressures or dam building.

Objectives

To assess the capacity of simplified models (i.e. those forced with a limited number of input data with a parsimonious structure and a few parameters to calibrate) to reliably simulate the thermal regimes of rivers, we tested three types of models. Two of these models are regression based, with equilibrium temperatures being determined by means of empirical air-to-water relationships (linear *vs* logistic), and the third is physically based, with the equilibrium temperatures being computed by the closure of the heat balance equation. These three categories of model are divided into several variants, depending on the following: (1) the computation of the heat exchange coefficient (constant, as a function of water temperature, and as a function of water temperature and wind speed) and (2) the computation of equilibrium temperatures (the variable number of input data and the method of computing long-wave incoming radiation). The testing domain is a plain river named the Middle Loire River, which is particularly well suited for this study, as it exhibits higher summer temperatures in recent records (>30 °C in August 2003) related to severe droughts (e.g. rainfall below 10 mm for August 2003 in the plain area) and very hot air temperatures (e.g. $T_a > 39\,°C$ in August 2003). Climate projections for the 21st century indicate increasing occurrences of hot and dry conditions compared with 2003 (Moatar *et al.*, 2010).

The main questions that are addressed in this paper are the following:

1. How do tested models perform in simulating the temperatures of a lowland river in terms not only of daily averages but also of seasonal fluctuations and heat peaks? Note that river temperatures are simulated at a daily time step, unlike previous studies that have used the equilibrium temperature concept and provided simulations under presumed stationary conditions at weekly time steps (e.g. Bogan *et al.*, 2004). Specifically, three methods for computing heat exchange coefficients are compared to assess their capabilities to account for the thermal inertia of the river.
2. How well are heat peaks simulated by each model? To address the individual sensitivity of each model variant to extreme hydrometeorological forcing variables, we performed two complementary analyses. The first approach uses observed water temperatures for the year 2003, which exhibited the warmest values (in air and water) in the last 35 years. The second analysis uses temperatures simulated by hydrological and thermal modelling that was forced with a climate change scenario based on a downscaled GCM projection of the A2 scenario of greenhouse gas release.

Overall, this analysis aims at determining the most reliable models for forecasting the impacts of climate change on the thermal regimes and heat peaks of temperate large rivers.

STUDY SITE

As the largest river in France, the Loire River is 1020 km long and drains a catchment area of 117 000 km^2 that is characterized by varying climates and lithologies. This river also experiences an irregular flow regime, including severe droughts. The monitoring station is at Avoine, which is located approximately 800 km downstream from the Loire River's source, approximately 340 km downstream from its confluence with the Allier River (14 300 km^2) and 30 km downstream from its junction with the Cher River (13 700 km^2). At this point, the Loire River drains an area of 60 000 km^2. It should be noted that because of the vicinity and morphological similarities of their lower reaches, the Cher River and the Loire River undergo comparable meteorological forcing conditions across the 100-km reach upstream from their confluence, thus leading to similar responses in terms of river temperature.

The water temperature for the upstream reach of the Middle Loire River is expected to be influenced by advective heat fluxes involving water with distinct thermal features that comes from upstream mountainous areas (e.g. Massif Central). In contrast, the intermediate and downstream reaches of the Middle Loire River, which are 340 km long and have a low river slope (approximately 25 cm/km) and an anabranching pattern (Claude *et al.*, 2012), are favourable for the convergence of water temperatures towards an equilibrium temperature. As the advective heat fluxes exert a notably slight influence on the thermal regime of the Loire River at its downstream reach, the station of Avoine appears well suited for comparing the performances of water temperature models that are based on the equilibrium temperature concept.

Although the temperature of the Middle Loire River is influenced mainly by thermal exchanges with the atmosphere, there are two additional heat sources that might diversely influence the thermal regime in the studied reach:

1. A heat flux related to river–groundwater exchanges (Gonzalez, 1993; Moatar and Gailhard, 2006) that involves the Beauce aquifer and the Val d'Orleans hydrogeological system (Albéric and Lepiller, 1998; Albéric, 2004). This flux is sensitive mostly between Orleans and Blois, and it can then be overlooked at Avoine *a priori*, as it is far downstream from the groundwater-fed reach (140 km).
2. The heat supplied by the cooling water from three nuclear plants located upstream from Avoine: St Laurent-des-Eaux (140 km upstream), Dampierre (230 km upstream), and Belleville (270 km upstream). This effect can also be neglected, as the nuclear power stations are equipped with closed-circuit cooling towers that allow the heat to be dissipated directly into the atmosphere. Thus, the thermal input into the Loire River is notably low, with a discharge averaging 2 m^3/s by product unit. Studies conducted by the electricity-generating authority (EDF) indicate that rises in daily temperature of the Loire River downstream from the Dampierre power station have a median of 0.1 °C and a 90th percentile of 0.3 °C, with the greatest increase being in winter.

The EDF provided the water temperature data for the station of Avoine, which is at an altitude of 35 m and is located a few hundred metres upstream from the warm water that is released by the nuclear power plant of Avoine–Chinon (Figure 1). The monitoring system consisted of a floating platform with a sensor that measured the water temperature at a depth of 20 cm (Moatar *et al.*, 2001). Examined and approved by EDF, the data allow for insight

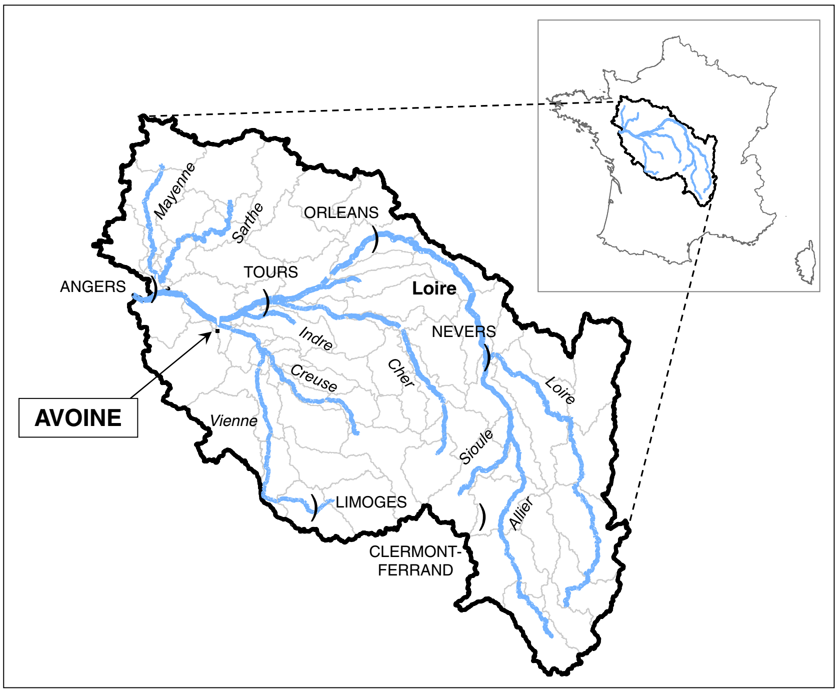

Figure 1. Map location of the study site of Avoine in the Loire River basin. The main hydrographic network and the delineation of the subwatersheds used for hydrological modelling are represented

into the impacts on river temperatures of warm water that has been released by three upstream power plants.

MODELS AND DATASET

Background theory

Assuming that the river is thermally well mixed and that there is no longitudinal temperature gradient, the energy budget equation can be expressed as

$$\frac{\partial T_{\mathrm{w}}}{\partial t} = \frac{\sum_i H_i}{\rho_{\mathrm{w}} \cdot Cp_{\mathrm{w}} \cdot D(t)} \tag{1}$$

where T_{w} is the river temperature, t is the time, ρ_w is the water density, Cp_w is the specific heat of the water, and $D(t)$ is the mean river depth at time t. The net heat flux ΣH_i, which results from the different heat exchanges across the air/water interface, was calculated by

$$\sum_i H_i = H_{\mathrm{ns}} + H_{\mathrm{la}} - H_{\mathrm{lw}} + H_{\mathrm{c}} - H_{\mathrm{e}} \tag{2}$$

where H_{ns} is the net solar radiation, H_{la} is the atmospheric long-wave radiation, H_{lw} is the long-wave radiation emitted from the water surface, H_{e} is the evaporative heat flux, and H_{c} is the convective (or sensible) heat flux exchanged with the atmosphere.

The equilibrium temperature concept

The equilibrium temperature (T_{e}) is the river temperature if the net heat flux across the river interface is 0:

$$\Sigma H_i = 0 \tag{3}$$

This net heat flux can be linearized as a function of equilibrium temperature (Edinger *et al.*, 1968) by stating that the net rate of heat exchange is proportional to the departure from the temperature equilibrium:

$$\sum_i H_i = K_{\mathrm{e}} (T_{\mathrm{e}} - T_{\mathrm{w}}) \tag{4}$$

The heat transfer coefficient K_{e} expresses the rate at which water temperature responds to the heat exchange processes. Combining Equations (1) and (4) leads to the following equation:

$$\frac{\partial T_{\mathrm{w}}}{\partial t} = \frac{K_{\mathrm{e}} \cdot (T_{\mathrm{e}} - T_{\mathrm{w}})}{\rho_{\mathrm{w}} \cdot Cp_{\mathrm{w}} \cdot D(t)} \tag{5}$$

Equation (5) indicates that the rate at which the water temperature approaches the equilibrium temperature varies proportionally to $K_{\mathrm{e}}/D(t)$. This formula is the fundamental equation for water temperature models that are based on the equilibrium temperature concept. The models that we tested (Table I) differ in their ways to compute T_{e} and K_{e} for solving T_{w}, which was calculated at a daily time step by

$$T_{\mathrm{w}}(t) = T_{\mathrm{e}}(t) + [T_{\mathrm{w}}(t - \Delta t) - T_{\mathrm{e}}(t)] \times \exp\left[\frac{-K_{\mathrm{e}}(t)}{\rho_{\mathrm{w}} \cdot Cp_{\mathrm{w}} \cdot D(t)} \times \Delta t\right] \tag{6}$$

where t is the time in seconds and Δt is the time step expressed in seconds. This equation presupposes that K_{e}, T_{e}, and D are constant over the time step of integration

Table I. Daily models based on the equilibrium temperature concept

Method	T_e computation	Data inputs	K_e^*		
			K1	K2	K3
Regression-based (RB)	Linear (L)	T_a	REG-L1-K1	REG-L1-K2	REG-L1-K3
		T_a, DL	REG-L2-K1	REG-L2-K2	REG-L2-K3
	Logistic (S)	T_a	REG-S1-K1	REG-S1-K2	REG-S1-K3
		T_a, DL	REG-S2-K1	REG-S2-K2	REG-S2-K3
Heat balance (HB)	$\Sigma H = 0$	Cld, R_g, U, RH, T_a	HB-ε_a-K1	HB-ε_a-K2	HB-ε_a-K3
		R_a, R_g, U, RH, T_a	HB-Ra-K1	HB-Ra-K2	HB-Ra-K3

(i.e. 1 day). Such a statement may seem dubious, especially during summer when diurnal fluctuations of T_e can be substantial. However, as a preliminary test, we compared simulations performed at daily and hourly time steps. Both thermal simulations provide comparable outputs in terms of mean daily water temperatures. The difference between both simulations is substantially reduced [a root mean square error (RMSE) of 0.31 °C instead of 0.58 °C] when a backward finite difference approximation is used for T_e, leading to the equation employed thereafter:

$$T_w(t) = \frac{[T_e(t) + T_e(t-\Delta t)]}{2} + \left[T_w(t-1) - \frac{T_e(t) + T_e(t-\Delta t)}{2}\right] \times \exp\left[\frac{-K_e(t)}{\rho_w \cdot Cp_w \cdot D(t)} \times \Delta t\right] \tag{7}$$

Finally, the accuracy of simulations that are based on the constant values of T_e, K_e, and D over the daily time step is acceptable, with a level of accuracy comparable with that of the recorded measurements (0.3 °C).

The heat exchange coefficient K_e. Three methods were used to compute the heat exchange coefficient K_e, which is as follows: (1) a theoretical formulation corresponding to the sum of derivatives of heat terms with respect to water temperatures, (2) an empirical linear relationship dependent on the water temperature, and (3) a constant value.

Following Edinger *et al.* (1968), the heat exchange coefficient K_e is theoretically determined by computing $-\sum_i \partial H_i / \partial T_w$, thus leading to

$$K_e(t) = 4.\varepsilon.\sigma \times (T_w(t) + 273.15)^3 + f(U) \times \left(0.62 + 6.11 \times \frac{17.27 \times 237.3}{(237.3 + T_w(t))^2} \times \exp\left(\frac{17.27 \times T_w(t)}{237.3 + T_w(t)}\right)\right) \tag{8}$$

where K_e is expressed as watt per square metre per Kelvin, Δt is the time step (s), and $f(U)$ is the wind function approximated by $f(U) = a_U \cdot U + b_U$ with a_U and b_U to be calibrated. To facilitate the interpretation of K_e, we computed the heat exchange coefficient for water, K_e^*,

$$Ke^*(t) = \frac{\Delta t}{\rho_w \cdot Cp_w} \times K_e(t) \tag{9}$$

where $\rho_w \cdot Cp_w = 4.181 \cdot 10^6$ J/m^3/K and K_e^* is given as metres per day with $\Delta t = 86\,400$ s, which corresponds to the rate at which T_w converges with T_e for a mean river depth of $D = 1$ m. For instance, $K_e^* = 0.5\,\text{m/day}$ means that $e^{-0.5} = 60.6\%$ of the thermal signal of the $(t-1)$th day is reported on the tth day if $D = 1$ m, but if $D = 5$ m, it reaches $e^{-0.5/5} = 90.5\%$. Preliminary tests indicated that Equation (8) tends to underestimate the thermal inertia of the water body, presumably because of the following: (1) the nonstationarity of air humidity above the river that is associated with evaporation processes and (2) the considerable weight given to wind speed, which is notably variable in space such that mean input data are not representative of local conditions (i.e. above the river) with respect to air turbulence (Morton, 1983). Moreover, the complementary relationship of the areal evapotranspiration model promoted by Morton (1983) posited that heat-induced turbulence is preponderant over wind-induced turbulence during periods of high evaporation. Thus, the evaporation loss can be viewed as much less sensitive to wind function. The heat exchange coefficient K_e^*, therefore, can be computed by using an empirical linear relationship that includes only the water temperature,

$$K_e^*(t) = a_K \cdot T_w(t-1) + b_K \tag{10}$$

where a_K and b_K are site-specific parameters to be calibrated and K_e^* is given as metres per day with $\Delta t = 86\,400$ s, which can thereby be directly introduced into Equation (6) for computing $T_w(t)$. Notice that we use the water temperature of the precedent day $(t-1)$ to avoid unnecessary iterative computations. This approach to compute the heat exchange coefficient is new because of the following: (1) the omission of the influence of the wind and (2) the calibration of the nature and magnitude of the control exerted by the water temperature T_w, instead of being inferred from the slope of the Clausius–Clapeyron relation (the second term of Equation (8)). Actually, Equation (8) presupposes that the air humidity (e_a) over a water body is independent of the river temperature, that is, $\partial(e_a)/\partial T_w = 0$. In light of the aforementioned preliminary tests, we consider that this assumption is questionable, at least, for the empirical equation we proposed, and that, by nature, this concept is much less adaptable to site-specific contexts. Third, and finally, we tested models with a constant K_e, as proposed earlier by Caissie *et al.* (2005).

The equilibrium temperature T_e. Three alternatives were considered for computing T_e: estimating T_e as linear or logistic functions of the air temperature T_a, which defines the so-called regression-based approaches, and solving for $\Sigma_i H_{i,j} = 0$, which is a nonlinear equation with an unknown river temperature $T_w(t)$ that is solved by means of the Newton–Raphson algorithm. The latter defines the heat balance approaches (also referred to as HB). Two subsets are distinguished depending on whether the atmospheric radiation is calculated after calibration or if it is extracted directly from the SAFRAN database (further details concerning these subsets are provided in the dedicated section 'Meteorological and Hydrological Datasets').

River depth D. To estimate the river depth, we analysed the gauging curves for the station of Langeais and 11 cross sections along the reach of the Middle Loire River, which led to the empirical relationship used thereafter that relates the mean river depth (D) with the river discharge (Q): $D = 0.10 \times Q^{0.50}$.

Tested thermal models

As alternatives to the reference simulation (or the REF), three categories of thermal model derived from the equilibrium temperature concept were tested. The designs of the simulations are presented in Table I. A distinction is first made between the models relying on the closure of the heat balance equation (HB-**-**) and the regression-based models (REG-**-**), which are further subdivided into linear and logistic models.

Regression-based approaches. Regression-based models estimate T_e according to the air temperature T_a. The subsequent relationship $T_e = f(T_a)$ can be either linear (models noted as REG-L*-**), as proposed by Caissie *et al.* (2005), or logistic (models noted as REG-S*-**), as inferred from Mohseni *et al.* (1998) and Bogan *et al.* (2004). The models of REG-L1-** are based on the hypothesis that T_e and T_a are linearly related,

$$T_e(t) = a_{TE}.T_a(t) + c_{TE} \tag{11}$$

where a_{TE} and c_{TE} are the parameters to be calibrated. Furthermore, to account for the seasonal variations of radiative input, we introduce an additional factor (day length factor, or DL) that is a function of the day length and that is expected to modulate the air/water temperature relationship for the models REG-L2-**,

$$DL(j) = \cos\left(\frac{2\pi}{365}\cdot(J + 193)\right) \tag{12}$$

with J representing the Julian day number corresponding to 1 (Jan 1) through 365 (Dec 31). The use of this proxy is a major original feature of this study. DL explains most (76%) of the radiative input variability (shortwave and infrared) but only 50% of the air temperature variability. Therefore, this variable can be viewed as a pertinent surrogate for radiative input when these data are not available and not as a superfluous additional one that provides redundant information with respect to air temperature. DL varies between -1 (for Dec 21) and +1 (for Jun 21). This factor is expected to account for the nonuniqueness of the $T_e = f(T_a)$ relationship, which is also influenced by incoming solar radiation. All other things being equal, the equilibrium temperature should be increasingly higher for the long-days/short-nights cycles because nighttime cooling is reduced. The equilibrium temperature is subsequently computed by means of a multilinear equation with three parameters,

$$T_e(t) = a_{TE}\cdot T_a(t) + b_{TE}\cdot DL(t) + c_{TE} \tag{13}$$

where a_{TE}, b_{TE}, and c_{TE} are site-specific calibrated empirical coefficients. Finally, for each model REG-L*-**, we test three distinct options to account for the thermal exchange coefficient K_e^*: the constant value (REG-L*-K1), the linear relationship using T_w as a covariate (REG-L*-K2), and the physically based formula (Equation (8)) for the models (REG-L*-K3).

The same protocol is applied to the models that are based on a logistic relationship of $T_e = f(T_a)$. For the models REG-S1-**, T_e is estimated by the following equation, which defines a S-shaped curve,

$$T_e(t) = T_n + \frac{T_x - T_n}{1 + \exp^{\gamma\cdot[\beta - T_a(t)]}} \tag{14}$$

where T_n and T_x are the lower and upper bounds of the water temperature, γ is the slope at the inflection point of the S-shaped curve defined by Equation (14), and β is the air temperature at the inflection point. These four parameters are site specific and must be calibrated. The consideration of the concomitant influence of the day length leads to the models RB-S2-**, with T_e computed as

$$T_e(t) = T_n + \frac{T_x - T_n}{1 + \exp^{\gamma\cdot[\beta - T_a(t)]}} + \lambda \times DL(t) \tag{15}$$

where λ is the coefficient that accounts for the influence of the day length.

The heat balance approach. The first step of the HB consists of calculating T_e as the hypothetical T_w for which incoming heat fluxes and outgoing heat fluxes are balanced (Equation (3)). The calculation procedures and related assumptions are presented in Table II. The main assumptions are as follows: (1) there is a temporally constant albedo of the water body (6%), (2) there is no light attenuation associated with riparian canopy and/or topographical features, (3) there is a temporally constant clear-sky atmospheric emissivity, following the prescriptions of Gras *et al.* (1986), Moatar (1997), and Gosse *et al.* (2008), and (4) there is an evaporation flux approximated

Table II. Rules for computing the five heat terms

Heat term	Calculation procedure	Assumptions	Calibration
Net solar radiation (H_{ns})	$H_{ns} = (1 - Alb) \times R_g \times (1 - SF)$	$Alb = 0.06$ (constant in time); $SF = 0$ (large river)	—
Atmospheric radiation (H_{la})	$H_{la} = 0.97 \cdot \varepsilon_a \cdot \sigma \cdot (T_a + 273.15)^4 \times (1 + 0.22 \cdot Cld^{2.75})$	ε_a = constant; $\sigma = 5.67 \cdot 10^{-8}$ W/m^2/K^4	ε_a
Long-wave emitted radiation (H_{lw})	$H_{lw} = 0.97 \cdot \sigma \cdot (T_w + 273.15)^4$	$\sigma = 5.67 \cdot 10^{-8}$ W/m^2/K^4	—
Convection (H_c)	$H_c = B \cdot f(U) \cdot (T_a - T_w)$	B = 0.62 mb/K; $f(w) = aW \cdot W + bW$	a_U and b_U
Evaporation/condensation (H_e)	$H_e = f(U) \cdot (e_{sw\text{-}ea})$	Magnus–Tetens approximation; $e_{sw} = 6.11 \times \exp[17.27 \cdot T_w/(237.3 + T_w)]$	

Alb, surface water albedo; R_g, global radiation (W/m^2); *SF*, shadow factor; ε_a, clear-sky atmospheric emissivity; T_a, air temperature (°C); *Cld*, cloud cover fraction; T_w, surface temperature of the water body; $f(U)$, wind function; e_a, water vapour pressure in air (mb); e_{sw}, saturation vapour pressure for T_w (mb).

by a Dalton-like equation with a calibrated wind function $f(U)$. Two categories of model are distinguished: those that use the atmospheric radiation data computed by SAFRAN and employ a radiative transfer scheme (Quintana-Segui *et al.*, 2008) as input data (HB-R_a-**) and those that compute these data by means of the Stefan–Boltzmann equation with a constant clear-sky atmospheric emissivity ε_a (HB-ε_a-**), as reported in Table II. As for regression-based models, three methods of computation for K_e were tested, which led to the test of $2 \times 3 = 6$ model variants based on the closure of heat balance equation.

Meteorological and hydrological datasets

Near-surface meteorological data. Long-term time series data for air temperature (T_a, 2 m above the soil surface in degree Celsius), specific humidity (*SH*, 2 m above the soil surface in kilogramme per kilogramme), wind velocity (U, 10 m above the soil surface in metres per second), global radiation (R_g, in watts per square metre), and atmospheric radiation (R_a, in watts per square metre) are provided by SAFRAN. SAFRAN is a gauge-based analysis system that combines atmospheric profiles from the global-scale reanalyses of the European Centre for Medium-Range Weather Forecasts with ground observations to provide time series of near-surface meteorological variables for climatically homogeneous zones (Vidal *et al.*, 2010). Optimal interpolation methods were implemented to provide hourly data covering France with an 8-km resolution for the period of 1970–2007. In contrast to the other variables, atmospheric radiation has not been validated because too few observations were available (Quintana-Seguí *et al.*, 2008). For simulations of the future, the same meteorological variables were obtained from the GCM Arpege (Gibelin and Déqué, 2003) as constrained by the extreme A2 scenario of anthropogenic emissions (Nakicenovic and Swart, 2000). The climatic scenario was simulated over the period of 1950–2100 with a variable resolution refined over Europe, which led to a resolution of approximately 50 km in the Loire River basin. This scenario was further downscaled to the resolution of the SAFRAN database with a weather regime approach (Boé *et al.*, 2006).

To force the thermal simulations, we used the arithmetic average of the cells that are comprised within the subwatershed containing the station, as weighted by the surface of each cell within the subwatershed. It should also be mentioned that the wind speed (U), provided at the 10-m height above the soil, was estimated at the 2-m height using a logarithmic wind profile, which led to $U_2/U_{10} = (2/10)^{0.11} = 0.837$.

Hydrological forcing. Discharge data were collected from the French HYDRO database (www.hydro.eaufrance.fr), which provided instantaneous and mean daily discharge values (m^3/s) and instantaneous river stages (in metres above sea level). The mean daily discharges used as input data for the present study are those measured at Langeais (20 km upstream from Avoine). When the data were missing or for climatic projections, the discharge was simulated by the semidistributed hydrological model EROS (Thiéry, 1988; Thiéry and Moutzopoulos, 1995) within 34 sub-watersheds (Figure 1) upstream from Avoine (Moatar *et al.*, 2010). Each of the subwatersheds is assumed to be homogeneous and is characterized in EROS by means of four to six lumped parameters (e.g. soil capacity and recession times) that were calibrated. The simulations of the mean daily discharge were performed over the periods 1970–2007 (forced by SAFRAN) and 1950–2100 (forced by the aforementioned downscaled climate scenario, referred to as Arpege A2 in the rest of the paper).

The calibration and validation of EROS were performed over the 1974–1990 and 1991–2007 periods, respectively, excluding 3 years (1971–1973) for initialization purposes. The agreement between the simulated and observed discharges is rather strong (Figure 2), with a Nash coefficient (computed with daily values) of 0.85 for the calibration period and 0.80 for the validation period, with a relative bias of 2%. EROS tends to underestimate peak flows and, to lesser extent, low-flow discharges. However, it should be noted that the errors on high flows do not have any significant influence on the outputs of 0D thermal models.

Regarding low flows below the tenth percentile of observed discharge, the errors remain moderate and are lognormally distributed with a right-skewed tail. Only 5% is underestimated by more than 40%, and 5% is overestimated by more than 76%. The fraction of discharge that is severely overestimated results from the model's tendency to anticipate rising water stages.

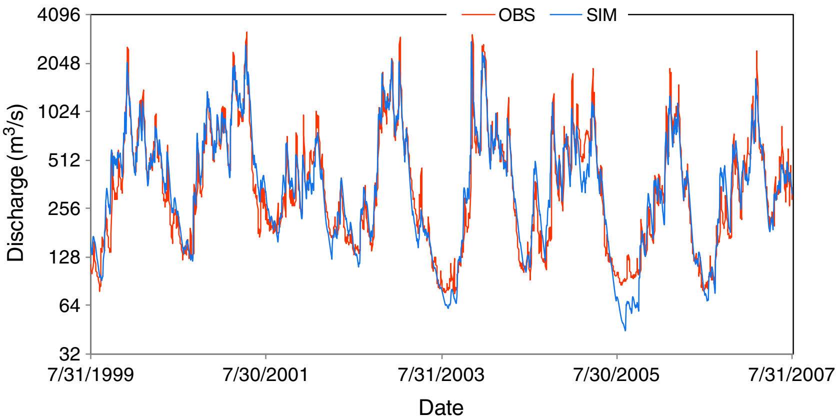

Figure 2. Simulated (SIM) and observed (OBS) discharge time series of the Loire River at the station of Chinon during 1999–2007. The simulated discharge was computed with the EROS hydrological model forced with the SAFRAN meteorological analysis

We also examined to what extent these errors in simulated discharge could influence the simulated water temperature. To this end, the reference model was forced either by observed discharge or by simulated discharge over the period 1976–2007. These two approaches lead to equivalent levels of performance (root mean square deviation = 0.17 °C) and patterns (not shown).

Design of the simulations

As a REF, Equation (1) was solved to simulate the temperature of the Loire River at Avoine, which was based on an hourly meteorological dataset and used a first-order finite difference explicit method at each hour. The hourly values were later averaged to allow for a comparison with the alternative thermal models that are presented hereafter and are based on the equilibrium temperature concept.

Apart from the REF, the simulations were performed at a daily time step. The simulation period was divided into two subdatasets: a calibration dataset that covered one third of the overall time series (sampled randomly for the period 1977–2007) and a validation dataset that covered the remaining years. The considered period, which covered 30 years (1/1/1977 to 7/31/2007), was marked by notably severe summer droughts (1976, 1989, 1990, 1991, and 2003) and several heat peaks (especially in 1997 and 2003). Very cold spells were observed in December 2001 and January 2003.

For calibration purposes, a Levenberg–Marquardt algorithm was employed to minimize the least squared error between the modelled values of the river temperature and the observed ones.

The performances of the models were assessed according to four performance criteria, as computed from the daily means of the observed and simulated temperatures for each season and during the entire analysis period:

1. The temperature mean bias (B_m), which is defined here for each Julian day by the difference between the simulated (T_w) and observed ($T_{w,OBS}$) river temperatures: $B_m = \bar{T}_w - \bar{T}_{w,OBS}$
2. The bias for the 90th percentile of the daily mean river temperature established for the whole dataset, which is represented by $B90 = T_w^{90} - T_{w,OBS}^{90}$
3. The bias for the 99th percentile of the daily mean river temperature established for the whole dataset, which is represented by $B99 = T_w^{99} - T_{w,OBS}^{99}$
4. The RMSE

COMPARED PERFORMANCES OF THE MODELS OF 1977–2007

Interannual scale

Calculated with daily values, the differences in RMSEs between the calibration and validation periods are notably low (with 1.00 °C for calibration *vs* 1.05 °C for validation, data not shown) and justify that model outputs from each subset are gathered and presented together. The general performances of the regression-based methods are notably strong despite their simplicity. The mean overall RMSEs for these models range between 0.90 and 1.27 °C (Table III).

In terms of performance, the hierarchy of methods is in strong agreement with what is expected. Regression-based methods are the least accurate, and heat balance methods provide better results if the clear-sky atmospheric emissivity is calibrated. The gain of performance when adding *DL* as a

Table III. RMSEs of the thermal models based on daily values with 18 variants based on daily time-step simulations and two on hourly time-step simulations (REF)

		RMSE			
Model	Data inputs	K1	K2	K3	REF
Linear	T_a	1.27	1.26	1.26	—
	T_a, *DL*	0.92	0.91	0.91	—
Logistic	T_a	1.24	1.23	1.23	—
	T_a, *DL*	0.90	0.90	0.90	—
Heat	*Cld*, R_g, *W*, *RH*, T_a	0.82	0.82	0.82	0.88
Balance	R_a, R_g, *W*, *RH*, T_a	1.07	1.07	1.06	1.04

Calibration and validation periods are gathered.
REF, reference simulation; RMSE, root mean square error.

covariate to regression-based models must be emphasized. In such cases, these methods are almost as efficient as the heat budget approach (HB), indicating that these simplified formulations enable the capture of nearly as much information as HB. This result also indicates that most of the water temperature variance is related to air temperature and day length. The REF (with the 0D heat budget equation directly being solved at the hourly time step) leads to an RMSE of 0.88 °C for the overall period when the atmospheric radiation is calibrated (fixed ε_a), which increases to 1.04 °C when using data for the observed atmospheric radiation (from the SAFRAN database). This finding suggests that the thermal simulations that use meteorological data at an hourly time step are not necessarily more accurate than those that are performed at a daily time step.

Seasonal patterns

The seasonality of errors is depicted by Figure 3. The differences that arise from the ways to compute K_e are notably small (Figure 3a) such that we only represented the errors for each model variant **-**-K1 and for the REF. Regression-based models that include air temperature as the only covariate exhibit the same pattern of error: water temperature tends to be severely underestimated in spring and overestimated in fall and winter (Figure 3b).

The method used to estimate the equilibrium temperature (linear *vs* logistic) seems of low importance in regard to patterns in mean error. When the Julian day is incorporated as a day length index and as a covariate to assess T_e, the seasonality of errors is fundamentally modified: water temperature is slightly overestimated in summer and is underestimated in fall (Figure 3c). The same pattern is found for the REF and for the heat balance models HB-**-K1 (Figure 3d). This common characteristic of REG-L2, REG-S2, HB, and the REF might be because of secondary heat inputs that are not accounted for in this study, such as streambed heat fluxes (Bogan *et al.*, 2004) that tend to buffer warming or cooling trends that are associated with climate forcing. Moreover, it should be noted that the reference and HB-ε_a-** simulations exhibit similar patterns of error, meaning that the time step of computation does not modify the model outputs substantially. In contrast, we observe a distinct pattern for HB-R_a-** that simulates lower than expected water temperature in winter, suggesting that the atmospheric radiation provided by the radiative transfer scheme may be underestimated.

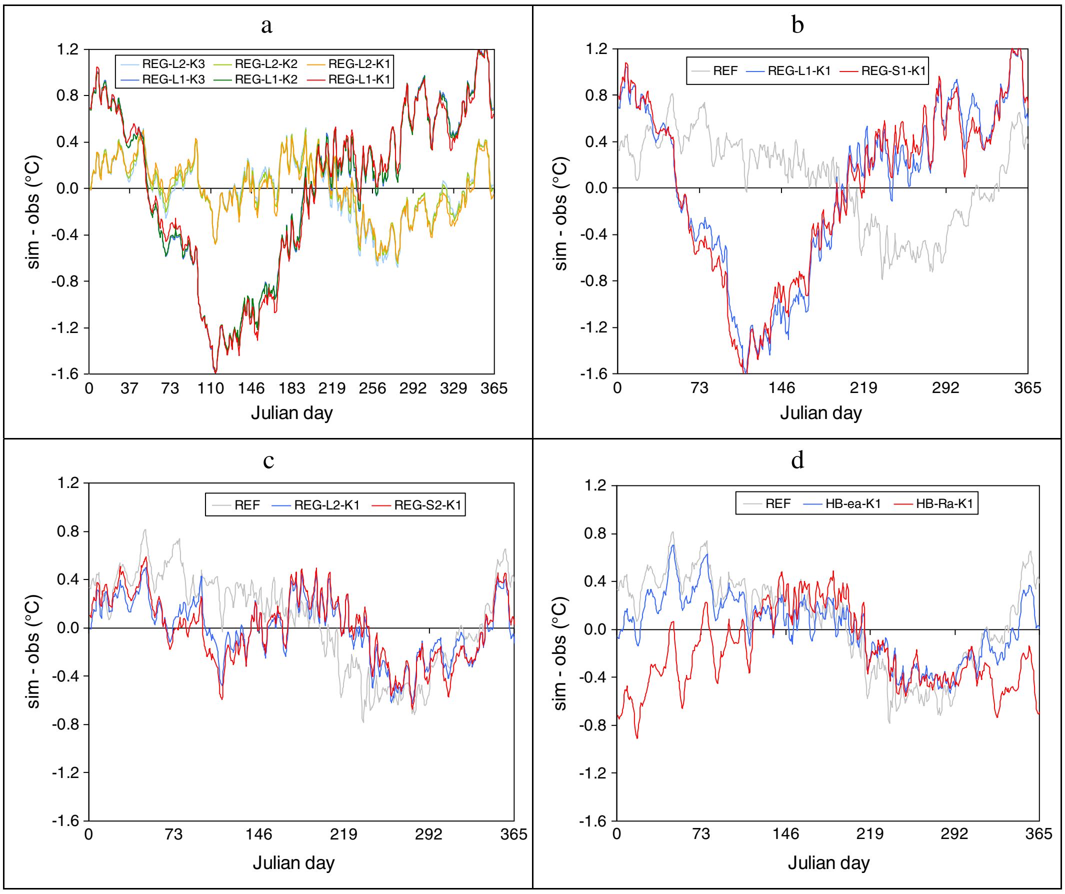

Figure 3. Seasonal structures of error ($T_w - T_{w,OBS}$, daily average by Julian day for the overall dataset, 1977–2007): (a) six regression-based variant models compared, with all combinations shown; (b) two regression-based variant models with constant K_e^* (REG-**-K1) and $T_e = f(T_a)$ estimated by linear (REG-L1-K1) and S-shaped (REG-S1-K1) relationships; (c) two regression-based model variants, with constant K_e^* and $T_e = f(T_a, DL)$ estimated by linear (REG-L2-K1) and S-shaped (REG-S2-K1) relationships; (d) and two heat balance models with a constant K_e^* and the atmospheric radiation computed by Stefan–Boltzmann's equation (HB-ε_a-K1) or by a radiative transfer scheme (HB-R_a-K1). The model variants presented in (b), (c), and (d) use a daily time step and are compared with the reference simulation (REF), which is performed at the hourly time step and uses the Stefan–Boltzmann's equation to compute the atmospheric radiation

Heat peaks

If air temperature is the only input data, the linear regression-based models largely overestimate the 99th percentile of temperature (T_w^{99}) (Table IV). Incorporating the day length as a second covariate (REG-L2-**) improves the simulations. However, the heat peaks (T_w^{90} and T_w^{99}) tend to be slightly underestimated for REG-S*-** (Table IV), as it is based on a logistic approximation of the equilibrium temperature as a function of air temperature. The incorporation of day length as a second covariate in these models does not influence the simulated temperature for heat peaks substantially.

The logistic function relating T_a and T_e implicitly mimics evaporation cooling, such that REG-S* models describe hot spells more accurately than do REG-L* models. The most accurate simulations are provided by the heat balance models. It also should be mentioned that the way to compute K_e^* does not strongly influence the thermal simulations, except for the REG-L* models, in which the tendency to overestimate water temperature is enhanced for REG-L*-K3 (the theoretical computation of K_e^*) and REG-L*-K2 (with a T_w-dependent relationship).

As a subsidiary test, we compared the thermal simulations of the 18 model variants for the summer of 2003 (Figure 4), recognized as the warmest ever recorded in France. First, the method to compute K_e does not seem to exert a strong influence on the simulated patterns of temperature. Considering a constant K_e over time tends to reduce the magnitude of variations compared with other computational strategies (K2 and K3), but this effect remains limited. Therefore, we consider five pools of model variants that provide comparable outputs for hot spells: REG-L1-**, REG-L2-**, REG-S*-**, HB-**-**, and the REF.

The regression-based models REG-L1-** overestimate the hottest temperatures by 1 to 3 °C, whereas those incorporating *DL* as a predictor of T_e, namely REG-L2-**, are in stronger agreement with observations (Figure 4a). In contrast, the regression-based models REG-S*-** (Figure 4b) tend to underestimate the magnitude of heat peaks. Finally, the heat balance models HB-**-** and the REF provide fair simulations of the river temperature for the summer of 2003 (Figures 3d and 4c), although the temperature tends to be slightly underestimated.

Calibrated parameters and their sensitivities

A crucial question regarding this methodology is whether the equilibrium temperatures that are estimated by linear (REG-L*-**) and logistic approximations (REG-S*-**) are consistent with those calculated more accurately by the HB.

Considering the heat exchange coefficient K_e^*, we obtain values ranging from 0.43 to 0.49 m/day for the **-K1 models (Table V). As the water temperature gets warmer, K_e tends to increase, as inferred from Equation (10). Depending on the water temperature, posited as between 0 and 32 °C, the heat exchange coefficient varies between 0.31 and 0.74 m/day when using Equation (10) (i.e. $K_e = f(T_w)$) and between 0.32 and 1.03 m/day for the theoretically derived K_e (Equations (8) and (9)), in consideration of a mean wind speed of 3.3 m/s. The discrepancies are larger at higher temperatures, which suggests that the actual thermal inertia of the river may depart from the theoretical one. This discrepancy might be due to the local air humidity over the water body, which limits the rate of evaporative loss.

Considering the equilibrium temperature for each category of REG-**-K* model, we find that the linear and logistic functions relating T_a and T_e are notably close (Table VI), regardless of the method of computation used for K_e^*. The incorporation of a second covariate to evaluate equilibrium temperatures, namely, *DL*, appears to be useful. The coefficient attributed to *DL* varies between 1.94 and 2.06, meaning that T_e, as it is computed from air-to-water

Table IV. Compared performances of the 18 tested models and the reference simulation (REF) over the period 1977–2007 and an outlook on hot spells with two criteria being investigated

Model	T_e	Bias	K_e^*		
			K1	K2	K3
Regression-based variant models	L1	B90	−0.2	−0.2	−0.2
		B99	0.3	0.5	0.6
	L2	B90	−0.2	−0.2	−0.2
		B99	−0.3	−0.1	−0.1
	S1	B90	−0.1	−0.1	−0.1
		B99	−0.4	−0.4	−0.4
	S2	B90	−0.1	0.0	−0.1
		B99	−0.4	−0.3	−0.4
Heat balance variant models	ε_a	B90	−0.1	−0.1	−0.1
		B99	−0.2	−0.1	0.0
	R_a	B90	0.0	0.0	0.0
		B99	−0.1	0.0	0.0
	REF	B90	−0.1		
		B99	−0.1		

B90 and B99 are the biases (°C) for the 90th and 99th percentiles of the daily mean river temperatures that were calculated for the entire year.
REF, reference simulation.

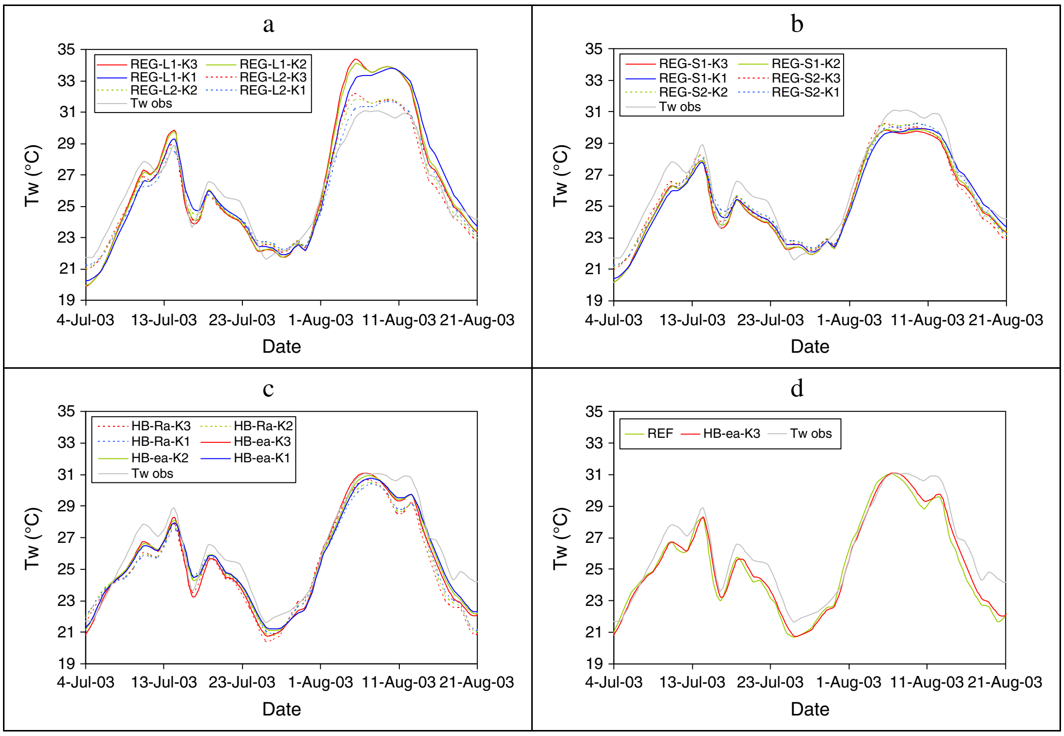

Figure 4. Water temperature of the Middle Loire River, as simulated by 19 model variants and observed for July–August 2003: (a) six regression-based model variants with a linear approximation of T_e; (b) six regression-based model variants with $T_e = f(T_a)$ estimated by S-shaped relationships; (c) six heat balance model variants with the atmospheric radiation computed by Stefan–Boltzmann's equation (HB-ε_a-K*) or by a radiative transfer scheme (HB-R_a-K*); (d) reference simulation (REF) based on 0D thermal model with a 1-h time step and a physically based heat balance approach (HB-ε_a-K3) with a 1-day time step. The model variants presented in (a), (b), (c), and (d) are compared with the mean daily observed temperature ($T_{w,OBS}$)

Table V. Computation of the heat exchange coefficient K_e^* for the 18 model variants tested

T_e computation	Data inputs	K_e^* (m/day)						
			K2 (Equation (10))			K3 (Equations (8) and (9))		
		K1	0 °C	13 °C	32 °C	0 °C	13 °C	32 °C
Linear	T_a	0.46	0.031	0.47	0.69	0.33	0.46	0.86
	T_a, DL	0.44	0.35	0.45	0.61	0.32	0.44	0.83
Logistic	T_a	0.49	0.32	0.49	0.74	0.34	0.48	0.90
	T_a, DL	0.46	0.38	0.47	0.60	0.33	0.46	0.86
Heat balance	Cld, R_g, U, RH, T_a	0.47	0.42	0.49	0.58	0.38	0.54	1.03
	R_a, R_g, U, RH, T_a	0.43	0.40	0.44	0.50	0.32	0.45	0.85

The theoretically derived K_e^* is obtained by applying Equation (8) with $U = 3.3$ m/s, which corresponds to the average wind speed observed for the studied period.

Table VI. Computation of the equilibrium temperatures T_e for the 12 regression-based tested model variants

$T_e = f(T_a)$	Data inputs	K_e^*	Calibrated equation
Linear	T_a	K1	$1.11 \times T_a + 0.84$
		K2	$1.11 \times T_a + 0.89$
		K3	$1.11 \times T_a + 0.89$
	T_a, DL	K1	$0.92 \times T_a + 2.06 \times DL + 3.16$
		K2	$0.92 \times T_a + 2.01 \times DL + 3.12$
		K3	$0.92 \times T_a + 2.03 \times DL + 3.18$
Logistic	T_a	K1	$-5.3 + 39.3/\{1 + \exp[0.12.(12.1 - T_a)]\}$
		K2	$-6.7 + 40.7/\{1 + \exp[0.12.(11.5 - T_a)]\}$
		K3	$-6.6 + 40.3/\{1 + \exp[0.12.(11.4 - T_a)]\}$
	T_a, DL	K1	$-6 + 42.8/\{1 + \exp[0.09.(13.4 - T_a)]\} + 2 \times DL$
		K2	$-6.2 + 42.8/\{1 + \exp[0.09.(13.1 - T_a)]\} + 1.94 \times DL$
		K3	$-7.3 + 43.7/\{1 + \exp[0.09.(12.4 - T_a)]\} + 1.98 \times DL$

equilibrium temperature relationships, should be corrected by -1.94 to $-2.06\,°C$ for winter solstice and by +1.94 to +2.06 °C for summer solstice.

When the HB approach is considered, the coefficients calibrated for the wind function (a_U and b_U) differ slightly from the values found elsewhere in the literature. We calculated $f(U) = 6.74 + 2.64\ U_2$ for HB-ε_a-** and $f(U) = 5.8 + 1.73\ U_2$ for HB-R_a-**, compared with, for instance, Penman's wind function of $f(U) = 7.4 + 4\ U_2$ from Brutsaert and Stricker (1979). This finding supports, at least partially, the aforementioned claim of Morton (1983) with respect to the specific microclimatic conditions presiding over large water bodies. Conversely, the clear-sky atmospheric emissivity ε_a is high (0.903). It is questionable whether atmospheric aerosols contribute to this enhancement of cloud emissivity (Garrett *et al*., 2002) and/or if a buffering mechanism is indicated, for example, the increasing contribution of secondary heat source inputs (in addition to the five heat terms) when the weather is cold. Several options are possible among which are the urban heat island effect and wastewater and/or industrial releases. It should also be mentioned that preliminary simulations conducted via empirical equations (e.g. Swinbank's equation: Swinbank, 1963) for estimating ε_a failed. Nonetheless, assuming a constant ε_a provides strong results and is consistent with the findings presented by Moatar (1997) and Gosse *et al*. (2008) for the Middle Loire River. This apparent stability of atmospheric emissivity might actually be observed because the temperature-dependent fluctuations of atmospheric emissivity were not balanced by the probable seasonality of cloud emissivity (higher in winter and lower in summer), as reported by Wylie and Menzel (1999) in the northern midlatitudes. For cloudy conditions, Malek (1997) noted substantial discrepancies between long-wave incoming radiation that was computed from Brutsaert's equation and from observations, relating them to the seasonal fluctuations of cloud-base height documented in Western Europe by Warren *et al*. (2007).

The heat exchange coefficient and its relation with microclimate. The poor quality of simulations obtained by computing the heat exchange coefficient from a theoretical formulation (Equation (8)) is striking. The empirical formulations that assume a linear relationship between K_e and T_w or a constant value enable better descriptions of the thermal inertia of the system. The range of variation of K_e obtained by the linear relation is 0.2–0.8 m/day, whereas the theoretical formulation leads to $0.3 < K_e^* < 1.2\ \text{m/day}$. This difference suggests that the reference model might overestimate the response of the river temperature to the variations of climate forcing. These findings are illustrated in Figure 5, in which hourly simulations from the REF exhibit smaller diurnal variations than observations from the very warm summer of 2003. In contrast, the diurnal variations of river temperature are well described for the summer of 2002 (Figure 5b), indicating that the way to compute K_e is perfectible and that the possible biased estimation of the river depth through $D = f(Qt)$ relationships cannot be invoked as the single possible cause.

In summer, the diurnal temperature ranges of the river (Figure 6, in which only 2001 and 2003 are presented) that are simulated by the reference model are occasionally well described (for 2001, 2002, and 2004), but they can also be largely overestimated (for 2003, 2005, and 2006). In our opinion, this variation might be due to the staticness of air humidity over the water surface in cases of high atmospheric stability. The heat exchange coefficient computed via Equation (8) implies that the air humidity above the river is constant in time. Given the width of the Loire River (>200 m), it is questionable to what extent the evaporation of the water might influence the local air humidity. In this specific microclimatic context, the sensitivity to warming phases might be sporadically lower than for turbulent well-mixed environments.

The empirical assessment of K_e^* partly enables an advancement over the approximations inherent to local retroactions. This process is of major interest to cases of large rivers, as it promotes the occurrences of very hot spells that are not observed in streams of lower size.

Given that a shift between the theoretical and empirical K_e^* is also found to a lesser extent in cold periods (i.e. when the evaporation is minimum), it can be hypothesized that other factors are operating. Among them, water exchanges between the river and the hyporheic zone and between the river and secondary channels of groundwater that are temporarily disconnected may explain, at least in part, the exceptionally long 'thermal memory' of the river. This

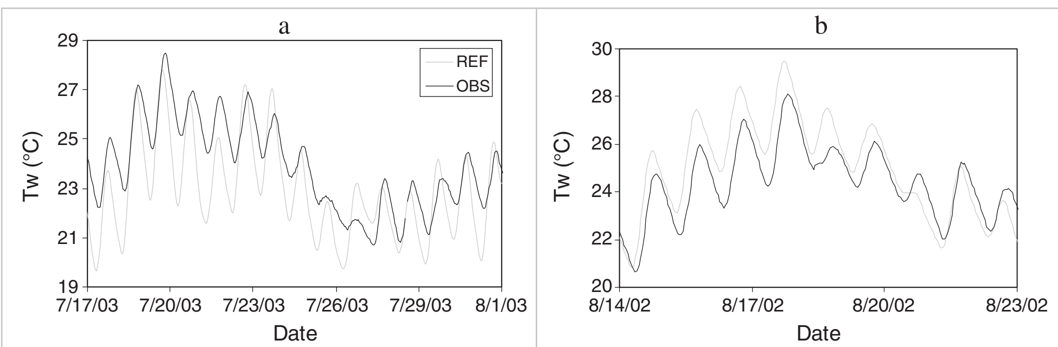

Figure 5. Simulated (REF) and observed (OBS) fluctuations of the river temperature at the hourly time step over a few days: (a) in summer of 2003 and (b) in summer of 2002. The simulated dataset is generated by the reference simulation and uses a 1-h time step

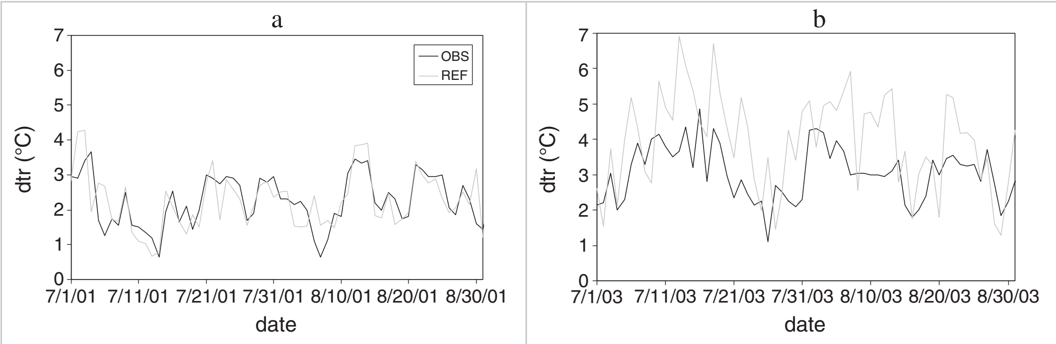

Figure 6. Simulated (REF) and observed (OBS) diurnal temperature ranges (dtr, °C) of the river temperatures for the summer period (July–August) of the years 2001 (a) and 2003 (b)

observation is consistent with the findings of Evans and Petts (1997), Burkholder *et al.* (2008), and Hannah *et al.* (2009) concerning the influence of the hyporheic zone not only on the thermal regimes of rivers but also on the longitudinal and transversal contrasts of temperature.

SIMULATED RESPONSES TO CLIMATE CHANGE

In this section, several model variants that were previously calibrated are applied to assess the impact of climate change on the temperature of the Loire River. The climate change forcing is continuous from 1950 to 2100, and the river temperatures were simulated for the entire time series (1950–2100), but we focus the analysis on the period 2081–2100, which is compared with the reference period (1971–1990). As suggested by the simulations for the present time, the method to compute the heat exchange coefficient does not greatly influence the models' outputs at the daily timescale. Hence, we only consider the model variants with constant heat exchange coefficients.

Mean impact of climate change

The changes in water temperature between the end of the 21st century (2081–2100) and the reference period (1971–1990) were analysed for each selected thermal model (Figure 7) and for the median values (T_w^{50}), 90th percentile (T_w^{90}), and 99th percentile (T_w^{99}).

Intermodel variability. Overall, the 18 model variants are mutually consistent for mean features and, especially, for low-temperature to moderate-temperature patterns. As the analysis focuses on extreme temperatures (e.g. T_w^{99} in summer), the models provide divergent outputs. Considering the median river temperature (T_w^{50}) in summer, it is noticeable that REG-L1-** leads to warming patterns distinct from the other models. This tendency is particularly the case in summer, in which the warming trend simulated by these models reaches 0.05 °C/year, whereas it remains inferior to 0.04 °C/year for any other model. This discrepancy between the linear regression models REG-L1-** and the other models increases for extreme temperatures. The inclusion of a second covariate to estimate the equilibrium temperature, leading to the models REG-L2-**, seems to overcome this deficiency, at least for the usual thermal

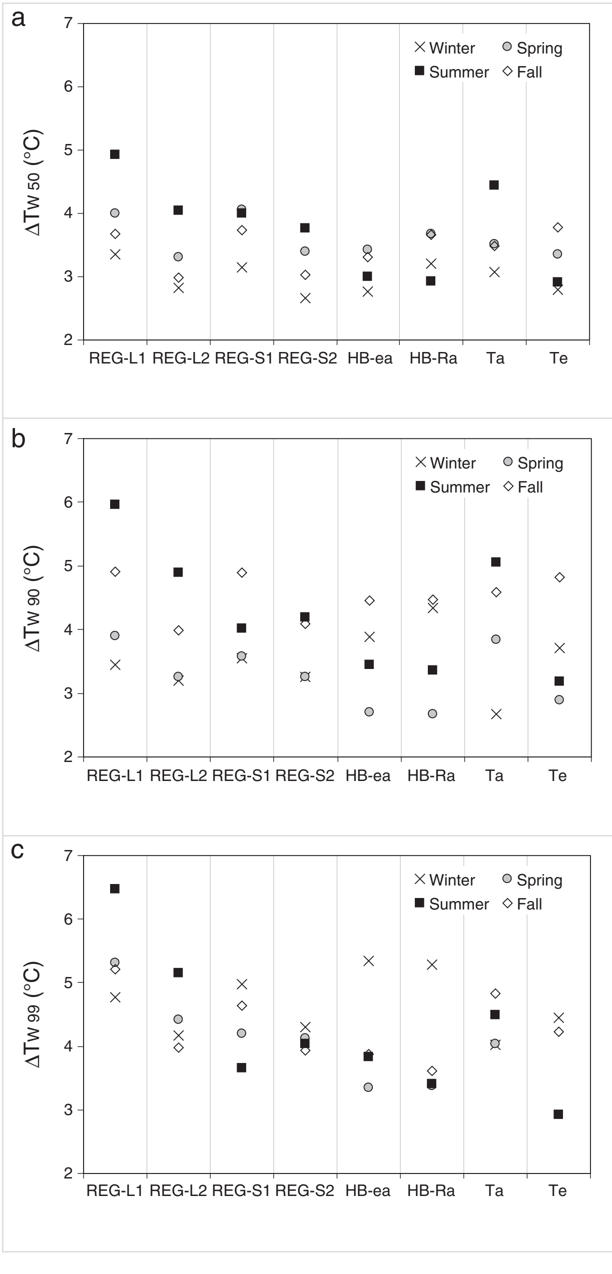

Figure 7. Anomalies in simulated water temperatures between 2081–2100 and 1971–1990 for the six thermal models with a constant K_e^* and for each season: (a) the median daily water temperature (ΔT_w^{50}), (b) the 90th percentile of T_w (ΔT_w^{90}), (c) the 99th percentile of T_w (ΔT_w^{99}). The last two columns in each panel show the anomalies between T_w^{50}, T_w^{90}, and T_w^{99} and the corresponding quantities for T_a and T_e

regimes. Above the 90th percentile in summer, the degree of difference between REG-L2-** and the more sophisticated models (REG-S*-** and HB-**-**) cannot be denied. The models that approximate the equilibrium temperature by means of a logistic relationship (REG-S*-**) are in stronger agreement with the heat balance models, more particularly for those that use day length as a second explaining variable (REG-S2-**). The REG-L* model variants, based on a linear T_e/T_a relationship, fail to accurately simulate the notably hot spells because of the 'evaporation cooling process' (Bogan *et al*., 2004) that dissipates an increasing part of excedentary energy via latent heat fluxes of high river temperatures. This flaw is attenuated for REG-S*-**, which is based on a logistic T_e/T_a relationship and leads to more realistic simulations for extreme forcing conditions. The simulations performed with the heat balance models (HB-**) are overall consistent with REG-S2-**, but they differ when the seasonal structure of the warming is considered.

Seasonal structure of the warming

By keeping the dubious simulations of the REG-L1 models apart, the overall magnitude of the warming is homogeneously distributed over the course of the year. The simulations indicate that this magnitude should represent up to 2 °C, regardless of the season. The models also simulate greater warming trends for infrequent events (at the 90th and 99th percentiles), probably because of the concomitance in the future of more frequent and drastic droughts (i.e. shallower water depths of −40%) with hotter atmospheric temperatures. However, the mean annual increase of river temperature (+2.2 to +3.5 °C) for the 2081–2100 period remains lower than the ones of air temperature (+3.6 °C) and of equilibrium temperature (+3.2 °C). This difference between air and water temperature increases for the hottest events corresponds to the 90th and 99th percentiles (Table VII).

To separate more accurately the contributions of the air temperature increases and the changes in the predicted flow regime, we performed additional simulations of water temperature over 2081–2100 using the downscaled Arpege A2 climate scenario as climate forcing and two distinct discharge datasets as hydrological forcing. Both approaches are based on the discharge simulated by the hydrological model EROS using Arpege A2 climate forcing for 2081–2100, but this discharge time series is unmodified in the first dataset (EROS), whereas in the second one (QQT), it is submitted to a quantile–quantile transformation to standardize the simulated discharge with the observed discharge in 1971–2007. This transformation withdraws the hydrological features that result from climate change forcing, such as the drastic decreases of the mean annual discharge (−55%) and of low flows (−70%) and the dampening of flood peaks. The simulated water temperatures that use these two discharge datasets provide useful indications for the specific contributions of flow regime changes on water temperature increases (Table VIII). In particular, when the EROS dataset that accounts for the full effect of the climate change scenario on river discharge is used, the simulated water temperatures tend to be warmer than if the climate change effect on river discharge is dampened (QQT).

The differences induced by the two discharge datasets tend to increase above the 90th percentile of water temperature, regardless of the season. However, the contribution of flow regime changes to increases in water temperature remains low. It never exceeds 15% (+0.6 over +4.0 °C in spring for the 99th percentile). On average, the difference between the water temperatures that are simulated with the two discharge datasets is 0.2 °C, which is less than 6% of the water temperature increase (+3.5 °C) simulated between 1971–2007 and 2081–2100. This finding suggests a weak sensitivity of water temperature warming to changes in flow regime, at least in the Middle Loire River.

Frequency distributions

Comparing the statistical distributions of water temperature between the historical and projected future periods enables a better understanding of potential changes in thermal variability, including the frequency of extreme values. The information obtained by means of the HB-ε_a-K1 model is synthesized in Figure 8, from which two points must be emphasized:

Table VII. The 50th, 90th, and 99th percentiles of T_a, the air temperature (from the Arpege v4 SRES A2); T_e, the equilibrium temperature (as computed from heat balance closure); Q, the discharge (m^3/s; from the hydrological model EROS); and D, the river depth (m) for three time horizons (1971–1990, 2046–2065, and 2081–2100) and their variations compared with the reference period (1971–1990: ΔT_a, ΔT_e, $\Delta Q/Q$, and $\Delta D/D$)

Quantile	Periods	T_a	T_e	Q	D	ΔT_a	ΔT_e	$\Delta Q/Q$ (%)	$\Delta D/D$ (%)
50	1971–1990	11.4	13.7	368	1.92	—	—	—	—
	2046–2065	13.6	15.8	235	1.53	2.3	2.1	−36	−20
	2081–2100	15.0	16.9	166	1.29	3.6	3.2	−55	−33
90	1971–1990	19.6	23.0	85	0.92	—	—	—	—
	2046–2065	22.1	24.6	50	0.70	2.5	1.6	−42	−24
	2081–2100	23.8	25.4	31	0.55	4.2	2.4	−64	−40
99	1971–1990	24.0	27.0	43	0.66	—	—	—	—
	2046–2065	26.7	28.4	24	0.49	2.7	1.4	−44	−25
	2081–2100	29.5	30.5	16	0.40	5.5	3.5	−63	−39

Table VIII. Water temperature simulated by the 18 thermal models for the period 2081–2100 for each season: (1) the median daily water temperature (T_w^{50}), (2) the 90th percentile of T_w (T_w^{90}), (3) the 99th percentile of T_w (T_w^{99})

	EROS				QQT				Anomaly			
	Winter	Spring	Summer	Fall	Winter	Summer	Spring	Fall	Winter	Summer	Spring	Fall
T_w^{50}	9.2	19.0	25.4	14.0	9.1	18.7	25.4	14.2	0.1	0.3	0.0	−0.2
T_w^{90}	13.4	23.8	28.2	20.6	12.8	23.4	27.9	20.7	0.6	0.4	0.3	−0.1
T_w^{99}	16.6	26.7	30.1	23.2	16.1	26.2	29.6	22.9	0.5	0.6	0.5	0.3
ΔT_w^{50}	3.0	3.5	3.8	3.5	2.9	3.4	3.8	3.6	0.1	0.2	0.0	−0.1
ΔT_w^{90}	3.5	3.3	4.1	4.5	3.2	3.0	3.9	4.5	0.3	0.3	0.2	0.0
ΔT_w^{99}	4.9	4.0	4.0	4.0	4.6	3.8	3.6	3.8	0.3	0.3	0.4	0.2

The thermal models are forced by two distinct discharge datasets that are based on the simulation by the hydrological model EROS over the 2081–2100 period, which is either unchanged (EROS) or smoothed by a quantile–quantile transformation (QQT). The water temperature changes between 2081–2100 and 1971–1990 are presented in the last three rows: ΔT_w^{50}, ΔT_w^{90}, and ΔT_w^{99} and their anomalies (EROS–QQT), depending on the discharge data that are used as hydrological forcing, are presented in the last four columns.

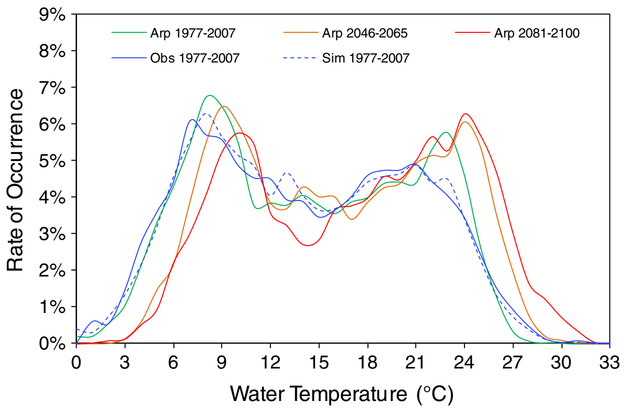

Figure 8. Statistical distributions (probability density function) of water temperatures in the Loire River at Chinon for historical and future periods. The simulations are performed with the HB-ε_a-K1 model. For the period 1977–2007, two simulations of water temperature are compared, one forced by SAFRAN (Sim) and another forced by the downscaled climate scenario (Arp). The observed probability density function over the same period is also presented (Obs)

1. In the historical period, the simulated water temperatures, whether forced by the SAFRAN database or by the downscaled climate scenario Arpege A2 for the period 1977–2007, show a bimodal distribution, such as with the observed water temperatures. However, the simulation forced by Arpege A2 exhibits substantial differences, especially for warmer temperatures, which are overrepresented between 22 and 25 °C and underrepresented above 25 °C.
2. When the distributions of water temperature simulated under the Arpege-A2 forcing between three successive periods (historical, middle of the 21st century, and end of the 21st century) are compared, a continuous drift towards warmer water temperatures with time is shown, but the change is not a mere translation. In the projected future, intermediate water temperatures (10–18 °C) are gradually less frequent, as are cold temperatures (the peak of occurrence centred at 6–9 °C decreases in magnitude), whereas the frequency of hot temperatures is enhanced. This shift results in a displacement of the main mode from 9 to 12 °C for the historical period towards 24 to 26 °C for the 2081–2100 period.

Taken together, these two points suggest that the thermal simulations that are performed under the climate change scenario Arpege A2 might underestimate water temperatures during the notably hot spells that may arise in upcoming decades. Note that this conclusion is model dependent and needs to be checked by alternative climate change scenarios that are based on different GCMs and/or downscaling methods.

CONCLUSION

In this study, the similarities and differences in modelled water temperatures were investigated for the following reasons: (1) to assess the robustness of simulated temperature trends, (2) to define their validity range, and (3) to define their transferability to future forcing conditions. Overall, the models based on the equilibrium temperature concept seem adequate for predicting the impact of anthropogenic climate changes, particularly for two reasons. First, their outputs, T_e and K_e, are climate derived and may be employed without reference to a historical time series of discharge, thus allowing the deconvolution of the impacts relative to the flow regime and to the meteorological changes of the river water temperature. Second, these models restrict the required input data for the calculation of T_e and K_e to those most reliably assessed by GCMs.

The regression-based models REG-L*-** and REG-S*-** are particularly interesting because of their parsimony in terms of the number of calibrated parameters and of the number of incoming forcing variables. These calculations might serve as decent models for cases when the air temperature and river discharge are the only available variables. These calculations are also suitable for assessing the impact of anthropogenic climate change because air temperature is the meteorological variable that is the most reliably predicted by GCMs (IPCC, 2007). These two models have many additional advantages, including their simplicity of use, lack of an annual bias, and moderate dispersion of errors. However, a penalizing flaw is identified for REG-L1-**, which is based on linear approximations of T_e by T_a and tends to overestimate highly during hot spells.

The transposition of REG-L1-** to projections of future periods for which hot thermal events are expected to be more frequent is thus not recommended. In comparison, regression-based models that rely on a logistic function between T_e and T_a (REG-S*-**) satisfactorily describe the hot spells, and their employment to simulate hot thermal sequences of the future reasonably can be recommended. This last method seems to offer the best compromise between performance and parsimony. It should be reminded that the equilibrium temperature is much better described when two covariates are used, namely, day length and air temperature, instead of the inclusion of only air temperature. The two covariates considerably limit seasonally structured errors that are observed when only T_a is employed as a covariate.

Overall, the studied heat balance models HB-**-** with five heat terms performed slightly better than the regression-based approaches. The main flaw of the five-term HB models studied was that they do not take into account the influence of secondary heat inputs, such as groundwater or anthropogenic heat inputs (whether implicitly, as for REG-L*-** and REG-S*-**, or explicitly, as for more elaborated models). This omission led to seasonally structured errors with an overestimated river temperature in spring and an underestimated river temperature in fall. This imperfection would probably be reduced by the inclusion of additional heat terms, such as streambed heat fluxes, which are potentially influenced by groundwater seepage.

It should also be reminded that the method for computing the heat exchange coefficient influences the magnitude of the heat peaks and the diurnal variability of water temperatures. Empirical formulas (K1 and K2) led to a considerable decrease of K_e, which enabled the simulation of highly realistic thermal responses in contrast to those obtained through a physically based formula. The empirical formulas avoid the overestimation of river temperatures during notably hot spells and considerably limit the seasonally structured errors, both of which are appealing for climate change studies.

In future periods, the river temperatures simulated by HB and REG-S2-** models exhibited similar variations and occurrences of hot spells over the 21st century at both the annual and seasonal scales. Despite variations in absolute terms, such as the differences between simulated river temperatures, these models provide convergent values in relative terms, including regarding the features and magnitudes of the variations of river temperature between time horizons (Figure 7). This result is important and indicates that simple approaches, such as regression-based models, might lead to the same results as more sophisticated models.

Finally, the most uncertain feature of the studied HB models regards their robustness under climate change scenarios, particularly because the models are forced with four meteorological variables (shortwave solar radiation, wind speed, relative humidity of air, and air temperature), which are subjected to a significant uncertainty in GCMs, even though the air temperature is predicted with a higher level of confidence than with other meteorological variables (Räisänen, 2007). Therefore, we warmly recommend assessing the impacts of climate change on river temperatures by means of regression-based methods that rely on logistic approximations of equilibrium temperatures T_e. This approach, which might perhaps be seen as crude, is actually at least as robust as the most refined classical heat balance models.

However, the question remains regarding to what extent the preceding analysis, focused on a rather large river reach, is transposable to the smaller headwater streams in which riparian shading, groundwater inputs, snowmelt, and sediment–water heat exchanges may be contributing significantly to stream heat budgets. A modified equilibrium temperature model that was based on HB and accounted for these additional heat terms was successfully implemented by Herb and Stefan (2011) to better estimate the thermal regime of cold-water streams. A generalization of our study to smaller streams could compare this type of model with the simplified regression-based models, which might be adapted by calibrating the empirical coefficients relating $T_e = f(T_a$, Julian day, shading factor) and $K_e = f(U)$ for rivers of variable size. This approach might offer an efficient way to regionalize river temperature models and/or to assess the magnitude of groundwater inputs for rivers.

ACKNOWLEDGEMENTS

This work was funded by the Fonds Européen de Développement Régional (FEDER) and the 'Etablissement Public Loire' by way of a postdoctoral fellowship associated to the project entitled ICC-HYDROQUAL-Impact du Changement Climatique sur l'hydrosystème Loire: HYDROlogie, Régime thermique, QUALité des eaux. Thanks are due to Météo-France for the SAFRAN database and the Arpege climate change projection. The two anonymous reviewers are acknowledged for their insightful comments that contributed to the improvement of the manuscript.

REFERENCES

Albéric P. 2004. River backflooding into a karst resurgence (Loiret, France). *Journal of Hydrology* **286**: 194–202.

Albéric P, Lepiller M. 1998. Oxydation de la matière organique dans un système hydrologique karstique alimenté par des pertes fluviales (Loiret, France). *Water Research* **32**: 2051–2064.

Bartholow JM, Campbell SG, Flug M. 2004. Predicting the thermal effects of dam removal on the Klamath River. *Environmental Management* **34**(6): 856–874. DOI: 10.1007/s00267-004-0269-5.

Bélanger M, El-Jabi N, Caissie D, Ashkar F, Ribi JM. 2005. Estimation de la température de l'eau en rivière en utilisant les réseaux de neurones et la regression linéaire multiple. *Revue des Sciences de l'Eau* **18**(3): 403–421.

Boé J, Terray L, Habets F, Martin E. 2006. A simple statistical–dynamical downscaling scheme based on weather types and conditional resampling. *Journal of Geophysical Research* **111**: D23106.

Bogan T, Stefan HG, Mohseni O. 2004. Imprints of secondary heat sources on the stream temperature/equilibrium temperature relationship. *Water Resources Research.* **40**: W12510. DOI: 10.1029/2003WR002733

Boisneau C, Moatar F, Bodin M, Boisneau P. 2008. Does global warming impact on migration patterns and recruitment of Allis shad (*Alosa alosa* L.) young of the year in the Loire River, France? *Hydrobiologia* **602**: 179–186.

Brutsaert W, Stricker H. 1979. An advection–aridity approach to estimate actual regional evapotranspiration. *Water Resources Research* **15**: 443–450.

Burkholder BK, Grant GE, Haggerty R, Khangaonkar T, Wampler PJ. 2008. Influence of hyporheic flow and geomorphology on temperature of a large, gravel-bed river, Clackamas River, Oregon, USA. *Hydrological Processes* **22**: 941–953.

Caissie D, El-Jabi N, St-Hilaire A. 1998. Stochastic modelling of water temperatures in a small stream using air to water relations. *Canadian Journal of Civil Engineering* **25**: 250–260.

Caissie D, Satish MG, El-Jabi N. 2005. Predicting river water temperatures using the equilibrium temperature concept with application on the Miramichi River catchments (New Brunswick, Canada). *Hydrological Processes* **19**: 2137–2159. DOI: 10.1002/hyp.5684

Caissie D, Satish MG, El-Jabi N. 2007. Predicting water temperatures using a deterministic model: Application on Miramichi River catchments (New Brunswick, Canada). *Journal of Hydrology* **336**: 303–315.

Chenard JF, Caissie D. 2008. Stream temperature modelling using artificial neural networks: application on Catamaran Brook, New Brunswick, Canada. *Hydrological Processes* **22**: 3361–3372.

Claude N, Rodrigues S, Bustillo V, Bréhéret JG, Macaire JJ, Jugé P. 2012. Estimating bedload transport in a large sand–gravel bed river from direct sampling, dune tracking and empirical formulas. Geomorphology, in press. DOI: 10.1016/j.geomorph.2012.07.030

Cluis D. 1972. Relationship between stream water temperature and ambient air temperature – a simple autoregressive model for mean daily stream water temperature fluctuations. *Nordic Hydrology* **3**(2): 65–71.

Ducharne A. 2008. Importance of stream temperature to climate change impact on water quality. *Hydrology and Earth System Science* **12**: 797–810.

Eaton JG, Scheller RM. 1996. Effects of climate warming on fish thermal habitat in streams of the United States. *Limnology and Oceanography* **41**: 1109–1115.

Edinger JE, Duttweiller D, Geyer J. 1968. The response of water temperatures to meteorological conditions. *Water Resources Research* **4**: 1137–1143.

Evans EC, Petts GE. 1997. Hyporheic temperature patterns within riffles. *Hydrological Sciences Journal* **42**(2): 199–213.

Gardner B, Sullivan PJ. 2004. Spatial and temporal stream temperature prediction: modelling nonstationary temporal covariance structures. *Water Resources Research* **40**: W01102. DOI: 10.1029/2003WR002511

Garrett TJ, Radke LF, Hobbs PV. 2002. Aerosol effects on cloud emissivity and surface longwave heating in the Arctic. *Journal of the Atmospheric Sciences* **59** (2): 769–778.

Gibelin AL, Déqué M. 2003. Anthropogenic climate change over the Mediterranean region simulated by a global variable resolution model. *Climate Dynamics* **20**: 327–339.

Giustolisi O, Doglioni A, Savic DA, Webb BW. 2007. A multi-model approach to analysis of environmental phenomena. *Environmental Modelling and Software* **22**: 674–682.

Gonzalez R. 1993. Etude de l'organisation et évaluation des échanges entre la Loire moyenne et l'aquifère des calcaires de Beauce. PhD thesis, Univ. d'Orléans, France.

Gosse P, Gailhard J, Hendrickx F. 2008. Analyse de la température de la Loire moyenne en été sur la période 1949 à 2003. *Hydroécologie Appliqueé* **16**: 233–274.

Gras RA, Gilbert A, Roult D. 1986. Numerical computation of natural river temperatures. In Proceedings of International Conference of Water Quality Modelling in Natural Environment. Bournemouth, 1–13 June, 457–472.

Gu R, Li Y. 2002. River temperature sensitivity to hydraulic and meteorological parameters. *Journal of Environmental Management* **66**: 43–56.

Hannah DM, Malcolm IA, Bradley C. 2009. Seasonal hyporheic temperature over riffle bedforms. *Hydrological Processes* **23**: 2178–2194. DOI: 10.1002/hyp.7256

Headrick MR, Carline RF. 1993. Restricted summer habitat and growth of northern pike in two southern Ohio impoundments. *Transactions of the American Fisheries Society* **122**: 228–236.

Herb WR, Stefan HG. 2011. Modified equilibrium temperature models for cold-water streams. *Water Resources Research* **47**: W06519. DOI:10.1029/2010WR009586

IPCC. 2007. Climate Change 2007 – the physical science basis. Contribution of Working Group I to the Fourth Assessment Report of the IPCC (ISBN 978 0521 88009-1 Hardback; 978 0521 70596-7 Paperback).

Johnson SL. 2003. Stream temperature: scaling of observations and issues for modelling. *Hydrological Processes* **17**: 497–499. DOI: 10.1002/hyp.5091

Kinouchi T, Yagi H, Miyamoto M. 2007. Increase in stream temperature related to anthropogenic heat input from urban wastewater. *Journal of Hydrology* **335**(1–2): 78–88. DOI:10.1016/j.jhydrol.2006.11.002

Mackey AP, Berry AD. 1991. The prediction of water temperatures in chalk streams from air temperatures. *Hydrobiologia* **210**: 183–189.

Malek E. 1997. Evaluation of effective atmospheric emissivity and parametrization of cloud at local scale. *Atmospheric Research* **45**: 41–54.

Moatar F. 1997. Modélisations statistiques et déterministes des paramètres physico-chimiques utilisés en surveillance des eaux de rivières: Application à la validation des séries de mesures en continu. Cas de la Loire moyenne. PhD thesis, Institut National Polytechnique de Grenoble, France; 290.

Moatar F, Miquel J, Poirel A. 2001. A quality-control method for physical and chemical monitoring data. Application to dissolved oxygen levels in the River Loire (France). *Journal of Hydrology* **252**: 25–36.

Moatar F, Gailhard J. 2006. Water temperature behaviour in the River Loire since 1976 and 1881. Comptes Rendus *Geoscience* **338**: 319–328.

Moatar F, Ducharne A, Thiéry D, Bustillo V, Sauquet E, Vidal JP. 2010. La Loire à l'épreuve du changement climatique. *Géosciences* **12**: 78–87. http://www.brgm.fr/dcenewsFile?ID=1306

Mohseni O, Stefan HG, Erickson TR. 1998. A non-linear regression model for weekly stream temperatures. *Water Resources Research* **10**: 2685–2692.

Mohseni O, Erickson TR, Stefan HG. 1999. Sensitivity of stream temperatures in the United States to air temperatures projected under a global warming scenario. *Water Resources Research* **35**(12): 3723–3733.

Moore RD, Sutherland P, Gomi T, Dhakal A. 2005. Thermal regime of a headwater stream within a clear-cut, coastal British Columbia, Canada. *Hydrological Processes* **19**: 2591–2608.

Morton FI. 1983. Operational estimates of areal evapotranspiration and their significance to the science and practice of hydrology. *Journal of Hydrology* **66**: 1–76.

Nakicenovic N, Swart R (eds). 2000. Intergovernmental Panel on Climate Change: Emissions Scenarios. Cambridge University Press, 599.

Poirel A, Gailhard J, Capra H. 2009. Influence de la gestion des barrages-réservoirs sur la température de l'eau. Exemple d'application au bassin versant de l'Ain. Proceedings SHF: Etiages, Sécheresses, Canicules rares, et leurs impacts sur les usages de l'eau. 8–9 Octobre 2009, Lyon, 8 p.

Poulin M. 1980. Modélisation du comportement thermique des cours d'eau, application au Rhin, Thèse de Docteur-Ingénieur, Université Pierre et Marie Curie et Ecole des Mines de Paris, Paris, 144 pp + annexes.

Quintana-Seguí P, Le Moigne P, Durand Y, Martin E, Habets F, Baillon M, Canellas C, Franchisteguy L, Morel S. 2008. Analysis of near surface atmospheric variables: validation of the SAFRAN analysis over France. *Journal of Applied Meteorology and Climatology* **47**: 92–107. DOI:10.1175/2007JAMC1636.1

Räisänen J. 2007. How reliable are climate models ? *Tellus A* **59**(1): 2–29. DOI: 10.1111/j.1600-0870.2006.00211.x

Sand-Jensen KAJ., Pedersen NL. 2005. Differences in temperature, organic carbon and oxygen consumption among lowland streams. *Freshwater Biology* **50**(12): 1927–1937. DOI: 10.1111/j.1365-2427.2005.01436.x

Sinokrot BA, Stefan HG, McCormick JH, Eaton JG. 1995. Modeling of climate change effects on stream temperature and fish habitats below dams and near groundwater inputs. *Climatic Change* **30**: 181–200.

Sivri N, Killic N, Ucan ON. 2007. Estimation of stream temperature in Firtina creek (Rize-Turkiye) using artificial neural network model. *Journal of Environmental Biology* **28**: 67–72.

Sridhar V, Sansone AL, LaMarche J, Dubin T, Lettenmaier DP. 2004. Prediction of stream temperature in forested watersheds. *Journal of the American Water Resources Association* **40**: 197–211.

St-Hilaire A, Morin G, El-Jabi N, Caissie D. 2000. Water temperature modeling in a small forested stream: implication of forest canopy and soil temperature. *Canadian Journal of Civil Engineering* **27**: 1095–1108.

Steel EA, Lange IA. 2007. Using wavelet analysis to detect changes in water temperature regimes at multiple spatial scales: effects of multi-purpose dams in the Willamette River Basin. *River Research and Applications* **23**: 351–359.

Stefan HG, Preud'homme EB. 1993. Stream temperature estimation from air temperature. *Water Resources Bulletin* **29**: 27–45.

St-Hilaire A, Morin G, El-Jabi N, Caissie D. 2003. Sensitivity analysis of a deterministic water temperature model to forest canopy and soil temperature in Catamaran Brook (New Brunswick, Canada). *Hydrological Processes* **17**: 2033–2047.

Swinbank WC. 1963. Longwave radiation from clear skies. *Quarterly Journal of the Royal Meteorological Society* **89**: 339–348.

Thiéry D. 1988. Forecast of changes in piezometric levels by a lumped hydrological model. *Journal of Hydrology* **97**: 129–148.

Thiéry D, Moutzopoulos C. 1995. Un modèle hydrologique spatialisé pour la simulation de très grands bassins: le modèle EROS formé de grappes de modèles globaux élémentaires. In: VIIIèmes journées hydrologiques de l'ORSTOM "Régionalisation en hydrologie, application au développement", Le Barbé et E. Servat (eds), ORSTOM Editions. 285–295.

Vidal JP, Martin E, Franchisteguy L, Habets F, Soubeyroux JM, Blanchard M, Baillon M. 2010. Multilevel and multiscale drought reanalysis over France with the Safran-Isba-Modcou hydrometeorological suite. *Hydrology and Earth System Sciences* **14**(3): 459–478.

Warren SG, Eastman RM, Hahn CJ. 2007. A survey of changes in cloud cover and cloud types over land from surface observations, 1971–96. *Journal of Climate* **20**(4): 717–738.

Webb BW, Nobilis F. 1997. Long-term perspective on the nature of the air–water temperature relationship: a case study. *Hydrological Processes* **11**: 137–147.

Webb BW, Walling DE. 1997. Complex summer water temperature below a UK regulating reservoir. *Regulated Rivers: Research & Management* **13**: 463–477.

Webb BW, Clack PD, Walling DE. 2003. Water–air temperature relationships in a Devon river system and the role of flow. *Hydrological Processes* **17**: 3069–3084. DOI: 10.1002/hyp.1280

Webb BW, Nobilis F. 2007. Long-term changes in river temperature and the influence of climatic and hydrological factors. *Hydrological Sciences Journal* **52**: 74–85.

Webb BW, Hannah DM, Moore RD, Brown LE, Nobilis F. 2008. Recent advances in stream and river temperature research. *Hydrological Processes* **22**: 902–918.

Wehrly KE, Brenden TO, Wang L. 2009. A comparison of statistical approaches for predicting stream temperatures across heterogeneous landscapes. *Journal of the American Water Resources Association* **45**(4): 986–997.

Wylie DP, Menzel WP. 1999. Eight years of high cloud statistics using HIRS. *Journal of Climate* **12**: 170–184.

